Composition-dependent structural and transport properties of amorphous transparent conducting oxides

Rabi Khanal,[1] D. Bruce Buchholz,[2] Robert P. H. Chang,[2] and Julia E. Medvedeva[1,*]

[1]*Department of Physics, Missouri University of Science & Technology, Rolla, Missouri 65409, USA*
[2]*Department of Materials Science and Engineering, Northwestern University, Evanston, Illinois 60208, USA*

Structural properties of amorphous In-based oxides, In-X-O with X = Zn, Ga, Sn, or Ge, are investigated using *ab initio* molecular dynamics liquid-quench simulations. The results reveal that indium retains its average coordination of 5.0 upon 20% X fractional substitution for In, whereas X cations satisfy their natural coordination with oxygen atoms. This finding suggests that the carrier generation is primarily governed by In atoms, in accord with the observed carrier concentration in amorphous In-O and In-X-O. At the same time, the presence of X affects the number of six-coordinated In atoms as well as the oxygen sharing between the InO_6 polyhedra. Based on the obtained interconnectivity and spatial distribution of the InO_6 and XO_x polyhedra in amorphous In-X-O, composition-dependent structural models of the amorphous oxides are derived. The results help explain our Hall mobility measurements in In-X-O thin films grown by pulsed-laser deposition and highlight the importance of long-range structural correlations in the formation of amorphous oxides and their transport properties.

PACS number(s): 81.05.Gc, 73.61.Jc, 71.23.Cq, 81.05.Ea

I. INTRODUCTION

Driven by technological appeal, the research area of amorphous transparent conducting oxides has grown tremendously since the first demonstration of the unique properties of these materials more than a decade ago [1,2]. Today, amorphous oxides of post-transition metals, such as indium-based ternary In-Sn-O (*a*-ITO) and In-Zn-O (*a*-IZO) or quaternary In-Ga-Zn-O (*a*-IGZO) and Zn-In-Sn-O (*a*-ZITO), exhibit optical, electrical, thermal, and mechanical properties that are comparable or even superior to those possessed by their crystalline counterparts, pushing the latter out of the market [3–6]. Yet, the structural variations associated with the crystalline-to-amorphous transition in these oxides are far from being understood. From experimental characterization, primarily via extended x-ray absorption fine structure (EXAFS) measurements [7–10] and from theoretical models derived from molecular dynamics (MD) simulations, it has been established that the first-shell characteristics—the average metal-oxygen distances and coordination—remain nearly intact upon the transition to the amorphous phase [11–20]. This suggests that, upon amorphization, both the optical band gap and the electron effective mass governed by the metal-oxygen interactions [21–23] should deviate only insignificantly from the crystalline values. Hence, the key features of the electronic band structure of a transparent conducting oxide host [24–26] should be preserved under the structural transition.

Recent investigations of amorphous indium oxide (*a*-IO) showed that the presence of nanocrystalline In_2O_3 inclusions whose size varies with deposition temperature limits the electron transport properties via scattering [10]. Nucleation of such nanocrystallites was found in amorphous In-O structures obtained via MD simulations at slow cooling rates (5 K/ps). Furthermore, the spatial distribution and interconnectivity of the fully coordinated In atoms, i.e., the InO_6 polyhedra, was shown to depend strongly on the quench rates in the MD

simulated structures. Based on a thorough comparison of the experimental and theoretical results, the observed peak in the electron mobility was found to correspond to the structure with long chains of the InO_6 polyhedra connected primarily via corner sharing [10]. Thus, the long-range structural characteristics, i.e., how the metal-oxygen polyhedra are integrated into a continuous network, play a key role in the transport properties of the amorphous oxides.

Amorphous transparent conducting oxides are compositionally adaptive and allow incorporation of large fractions of other post-transition metals, e.g., Sn, Zn, or Ga, into the In-O matrix. The presence of additional cations affects the crystallization temperature and often makes it easier to achieve an amorphous state of the multicomponent oxide. Yet the microscopic effect of the composition on the local and long-range structural characteristics of amorphous In-based oxides as well as on their transport properties—carrier generation, carrier concentration, and carrier mobility—is still unclear.

In marked contrast to the crystalline transparent conducting oxides, where the electron mobility is governed primarily by the scattering on the ionized or neutral impurities, phonons, and grain boundaries, the local distortions of the metal-oxygen polyhedra and the long-range structural disorder in amorphous oxides makes their transport properties more complex. Although amorphous oxides lack grain boundaries, additional electron scattering is expected to occur due to (i) size and spatial distribution of the nanocrystalline inclusions; (ii) spatial distribution and clustering of incorporated cations in multicomponent oxides; (iii) abundant trap defect states; and (iv) piezoelectric effects associated with internal strains. Clearly, chemical composition, oxygen deficiency, as well as deposition temperature will have a strong effect on the above processes and should be systematically investigated.

In this work, we present a systematic study of the structural properties of ternary amorphous In-based oxides, In-X-O with X = Zn, Ga, Sn, or Ge, denoted below as *a*-IXO, obtained via liquid-quench MD simulations. To gain a thorough understanding of the role of composition in the structural properties of the amorphous oxides, the characteristics of the

*juliaem@mst.edu

first, second, and third shells are compared between amorphous indium oxide, ternary a-In-X-O, as well as the corresponding crystalline oxides. In addition to the average distances and coordination numbers from the standard pair distribution functions, statistical distributions and weighted averages as a function of cation number and/or type of oxygen sharing are presented. The results reveal the importance of long-range structural correlations governed by the composition and explain the observed carrier concentration and mobility trends in amorphous In-X-O. All results presented in this work are for stoichiometric oxides; the effect of oxygen nonstoichiometry, important for the defect formation, carrier generation, and carrier transport in amorphous oxides [16,27–32], will be discussed in a future study.

II. COMPUTATIONAL METHOD

The amorphous a-In-O and a-In-X-O structures were generated using first-principles molecular dynamics as implemented in the Vienna Ab Initio Simulation package (VASP) [33–36]. The calculations are based on the density functional theory (DFT) [37,38] with Perdew-Burke-Ernzerhof (PBE) functional within the projector augmented-wave method [39–41]. For the initial structure, we used a cubic 130-atom cell of bixbyite In_2O_3 with density 7.12 gm/cm^3. To obtain ternary In-X-O structures, we randomly replaced 20% of the In atoms in the initial structure by respective metal X (Zn, Ga, Sn, or Ge) and adjusted (i) the number of oxygen atoms to maintain stoichiometry (as well as charge neutrality), and (ii) the cell volume to maintain the density in the In-based samples. For each initial In-O or In-X-O structure, we performed molecular dynamics simulations of liquid quench as follows. First, to remove any crystalline memory, each initial structure was melted at 3000 K for 6 ps. The melt was then cooled to 1700 K at the rate of 100 K/1.2 ps, and then rapidly quenched to 100 K at the rate of 200 K/1.2 ps. In order to make the calculations computationally efficient, we used low cutoff of 260 eV and restricted the k-point sampling to Γ point only during melting and quenching processes. Finally, each structure was equilibrated at 300 K for 6 ps with a cutoff energy of 400 eV. All simulations were carried out within NVT ensemble with Nosé-Hoover thermostat using integration time step of 2 fs.

III. GROWTH AND CHARACTERIZATION

Amorphous oxide thin films were grown by pulsed-laser deposition (PLD) from a dense hot-pressed indium oxide, zinc oxide, tin oxide, and gallium oxide targets (25 mm diameter). PLD was accomplished with a 248 nm KrF excimer laser with 25 ns pulse duration and operated at 2 Hz. The 200 mJ/pulse beam was focused onto a 1 mm × 2 mm spot size. The target was rotated at 5 rpm about its axis to prevent localized heating. The target-substrate separation was fixed at 10 cm. For multicomponent films the appropriate basis-oxide targets were employed. A computer controlled shuttle was used to alternate ablation between targets. Less than one monolayer of material was deposited in a typical cycle between the targets to help ensure uniformity of film composition; the ratio of the pulses for each metal oxide in each cycle was adjusted to obtain the desired film composition. The compositions reported are nominal compositions: the ratio of the number of dopant pulses to total pulses. The films were grown on silicon substrates in an O_2 ambient of 8 mTorr. The substrates were attached to the substrate holder with silver paint and grown at a temperature of $-25\,^\circ$C to ensure amorphous films.

Sheet resistance (R_s: $\Omega/\square$), carrier type, area carrier-concentration (n_a: 1/cm^2), and carrier mobility (μ_{hall}: cm^2/V s) were measured with a Ecopia 3000 Hall measurement system on samples in the van der Pauw geometry. Carrier density (n_v: 1/cm^3) and resistivity (ρ: Ω cm) were calculated by dividing the area carrier concentration and sheet resistance, respectively, by the film thickness. Film thickness (d: nm) was measured using a spectral reflectometer (Filmetrics F20) and was shown to range 250–300 nm.

IV. RESULTS AND DISCUSSION

A. Local (short-range) structural characteristics

1. In-O distances in amorphous In-O and In-X-O

To understand how composition affects the structural properties of amorphous In-based oxides, we first analyze the local structure of the InO_x polyhedra, i.e., the In-O distances and the coordination of In with oxygen atoms. The results are compared to the corresponding values for In-O in a-In-O and then to those for X-O values in a-In-X-O, X = Zn, Ga, Sn, or Ge.

The radial In-O distribution functions in a-In-O and a-In-X-O show insignificant variation in the width and peak position for different X; Fig. 1. The calculated standard deviation, σ^2, for the first-shell distances slightly increases from 0.011 Å^2 for a-In-O and a-IZO to 0.012 Å^2 for a-IGO, and to 0.013 Å^2 for a-ITO and a-IGeO. Despite the different ionic radii of the X cations, the average In-O distance is similar in a-In-O and all a-In-X-O. For a more accurate comparison of the average In-O distances in a-In-O and a-In-X-O the average pair correlation
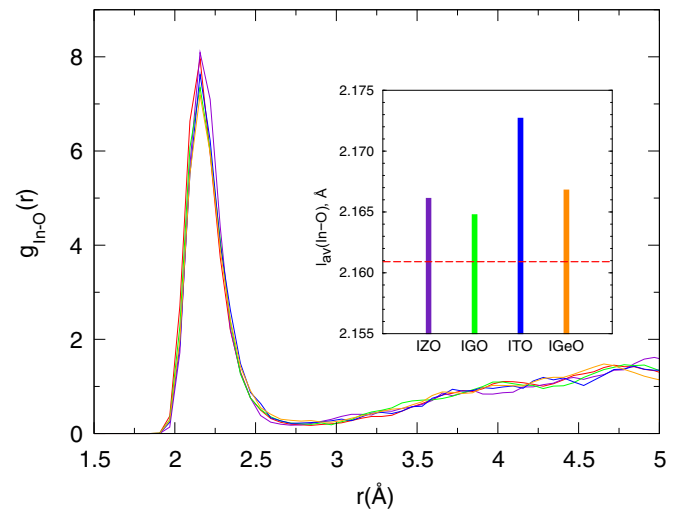

FIG. 1. (Color online) Radial In-O pair distribution functions in amorphous In-O and In-X-O. In the inset, the calculated average In-O pair correlation function, l_{av}, is plotted for amorphous In-X-O. The horizontal dash line represents the corresponding l_{av} value in amorphous In-O.

function [42,43] is calculated according to

$$l_{av} = \frac{\sum_i l_i \exp\left[1 - \left(\frac{l_i}{l_{min}}\right)^6\right]}{\sum_i \exp\left[1 - \left(\frac{l_i}{l_{min}}\right)^6\right]}, \qquad (1)$$

where the summation runs over all oxygen neighbors of a particular In atom and l_{min} is the smallest In-O distance in the ith InO$_x$ polyhedron. The average pair correlation function is weighted by taking into account the individual metal-oxygen bond lengths, and eliminates the long-distance bonds that represent noninteracting M-O pairs. The results, given in the inset of Fig. 1, reveal that the average pair correlation function increases from 2.161 Å for a-In-O to 2.165 Å for a-IGO; 2.166 Å for a-IZO; 2.167 Å for a-IGeO; and to 2.173 Å for a-ITO. Hence, the addition of X cations leads to a slight increase of the average In-O distance which remains to be below the corresponding value in crystalline In$_2$O$_3$, namely, 2.18 Å.

To further understand the effect of X on the first-shell In-O distances, the average In-O distance (l_{av}) is calculated as a function of the number of X atoms in the second shell of the In atoms. For this, for every indium atom, the number of X nearest neighbors, i.e., those located within a sphere of radius 3.4 Å, is determined. The latter corresponds to the In-In distance in c-In$_2$O$_3$. There may be no, one, two, three, or four X neighbors in the second shell of an In atom; the number of In atoms in each of the groups is given as a percent of the total number of In atoms in the cell; cf., Table I. The average pair correlation functions [Eq. (1)] were then calculated for each of the In groups. First of all, it is found that for indium atoms with no X neighbors in the second shell, the calculated average In-O pair correlation function differs from the one in a-In-O ($l_{av} = 2.161$ Å) being larger for $X =$ Zn or Sn ($l_{av} \sim 2.176$ Å), and smaller for $X =$ Ga or Ge ($l_{av} \sim 2.154$ Å), Table I. The ionic size of the former two cations (Zn and Sn) is larger than that of the latter two (Ga and Ge); in addition, the strength of the X-O bonds is weaker in the former case compared to the latter case. Hence, one can argue that Ga and Ge, having short and strong bonds with their neighboring oxygen atoms, increase the In-O distance of their nearest-neighbor In atoms. As a result of such "oxygen-getter" behavior [44], the In-O bond length for In atoms that are farther away from Ga and Ge cations decreases.

Different mechanism(s) should be sought for a-IZO and a-ITO because the ionic size of Zn or Sn is smaller compared to that of In; and the metal-oxygen bond strength is similar for

In, Zn, and Sn. In the case of a-IZO, the longer In-O distances for the In atoms that do not have a Zn atom in the second shell, Table I, are likely to originate from an increased average In-O coordination away from Zn: the average In coordination for the In atoms that do not have a Zn neighbor is $\sim$5.4 that is notably higher than for a-In-X-O with $X =$ Sn, Ga, or Ge, Table I, or for a-In-O where the average In coordination is $\sim$5.0. In a-ITO, a strong preference of Sn atoms toward natural coordination and clustering discussed in the sections below may lead to longer In-O distances away from Sn. Clustering of Sn atoms is already evidenced from the large number, 48%, of the In atoms with no Sn neighbor in the second shell as compared to all other cases, Table I.

When the number of X nearest neighbors for a particular In atom increases, the average In-O distance behaves differently in a-In-X-O. In the case of $X =$ Zn, the In-O pair-correlation function decreases with the number of second-shell X neighbors, Table I. Significantly, the average In-O distance for the In atoms with two or three Zn nearest neighbors is nearly equal to that found in crystalline In$_2$ZnO$_4$, 2.154 Å. In contrast to a-IZO, there is no consistent trend for the In-O distances for $X =$ Ga, Sn, or Ge, Table I. This may be explained by (i) comparable bond strengths for Zn-O and In-O as opposed to those for Ga-O and Ge-O; and (ii) the fact that Zn atoms are uniformly distributed throughout the In-O matrix—in marked contrast to Ge, Ga and especially Sn atoms that show a strong tendency to cluster (as discussed in more detail in Sec. IV B 3). The strong Ga-O and Ge-O bonds tend to increase the In-O distances as the number of Ga or Ge nearest neighbors increases (with an exception for the case of two X atoms, Table I, which we attribute to a particular spatial distribution of the two X atoms, e.g., a possibility for X-X dimer formation). The above findings are consistent with crystalline multicomponent oxides: the average In-O distance in GaInO$_3$ (2.174 Å) and In$_2$Ge$_2$O$_7$ (2.163 Å) is longer as compared to that in In$_2$ZnO$_4$ (2.154 Å).

Among the X cations considered in this work, tin results in the largest average In-O distance, Fig. 1. At the same time, the least variation in the average In-O distances is observed in a-ITO: independent of the number of Sn nearest neighbors, the average In-O distance remains close to the overall average, 2.173 Å, Table I. As will be shown in Sec. IV A 3, the presence of tin has the least effect on the In-O coordination statistics, i.e., the numbers of differently coordinated In atoms

TABLE I. Average In-O pair correlation function, l_{av} in Å, and effective coordination number, ECN (In-O), cf. Eq. (2), as a function of the number of X atoms, NN_X, located within the radial distance of 3.4 Å from a central In atom. The fractional number of the In atoms, N_{In}, in percent, that have a certain number of X neighbors in the second coordination sphere, i.e., with $NN_X = 0$, 1, 2, 3, or 4, is given in brackets. The total average pair-correlation function, $\langle l_{av} \rangle$, and total average effective coordination number, $\langle$ECN(In $-$ O)$\rangle$, are given in the last column. For comparison, the average In-O pair-correlation function is 2.161 Å and the average In-O effective coordination number is 5.0 in a-In-O.

| | l_{av}, ECN (In-O) (N_{In}) | | | | | |
NN_X	0	1	2	3	4	Average
IZO	2.177, 5.4 (20)	2.170, 5.1 (46)	2.156, 5.0 (27)	2.151, 5.1 (7)		2.166, 5.1
IGO	2.156, 5.0 (30)	2.174, 5.2 (46)	2.149, 5.0 (20)	2.199, 6.2 (2)	2.198, 5.2 (2)	2.165, 5.1
ITO	2.175, 5.1 (48)	2.168, 5.1 (41)	2.180, 5.5 (11)			2.173, 5.1
IGeO	2.153, 5.1 (30)	2.172, 5.3 (50)	2.144, 5.2 (11)	2.213, 5.8 (9)		2.167, 5.3

remain unchanged upon introduction of tin. Indeed, the ionic size, bond strength, and preference for six-fold coordination with oxygen atoms are similar for In and Sn—in accord with the presence of fractional site occupation for Sn and In in crystalline $In_4Sn_3O_{12}$ and other crystalline oxides that contain In and Sn. Hence, one needs to look beyond the local, short-range structural features of amorphous oxides in order to explain the increase of the average In-O distance in a-ITO with respect to a-In-O. Indeed, the spatial distribution and connectivity of SnO_x and InO_6 polyhedra in a-ITO provide a plausible explanation; see Sec. IV B 3.

Thus, although all X cations considered in this work result in a slightly increased average In-O distance, a thorough structural analysis suggests that the origin of the X effect is different in a-In-X-O. Longer In-O distances are expected to increase the electron effective mass and, hence, may contribute to the reduced mobility in amorphous In-X-O as compared to amorphous In-O. However, the obtained changes in the In-O distances are not significant enough to explain the observed mobility reduction as the fraction of X increases. We believe that the transport properties in amorphous oxides are governed by spatial distribution and connectivity of the MO_x polyhedra, i.e., the long-range features of the amorphous structure, rather than the local M-O bonds.

2. X-O distances in amorphous In-X-O

The radial X-O pair distribution functions in a-In-X-O are shown in Fig. 2. Also, the calculated average pair correlation function $l_{av}(X$-O$)$, Eq. (1), for each a-In-X-O structure is given in the inset of Fig. 2. The results reveal that for $X =$ Sn or Ge (for $X =$ Zn or Ga), the average X-O distance is shorter (longer) than the natural X-O distance, i.e., the distance in the corresponding crystalline binary oxides. The same trend is found when the average X-O distances are compared for crystalline binary and crystalline ternary oxides. The Sn-O and Ge-O distances are shorter in the ternary oxides with In: the

average Sn-O distances are 2.06 and 2.09 Å in $In_4Sn_3O_{12}$ and SnO_2, respectively; the average Ge-O distances are 1.74 and 1.88 Å in $In_2Ge_2O_7$ and cristobalite/rutile GeO_2, respectively. The Zn-O and Ga-O distances are slightly longer in the ternary oxides with In: the average Zn-O distances are 1.99 and 1.98 Å in In_2ZnO_4 and wurtzite ZnO, respectively; and the average Ga-O distances are 1.94 and 1.93 Å in $GaInO_3$ and Ga_2O_3, respectively [45].

Significantly, in the case of Zn addition, the radial Zn-O distribution features a nonzero tail at longer distances, i.e., there is an appreciable amount of long-distance Zn-O bonds in a-IZO, Fig. 2. In contrast, the radial distribution functions for $X =$ Ga, Sn, or Ge are narrow, with the calculated standard deviation $\sigma^2 < 0.001$ Å^2, and vanish above ~2.4 Å, Fig. 2. Thus, comparing the shape of the radial X-O pair distribution function for a-In-X-O, we conclude that Zn in amorphous In-Zn-O allows for both shorter and longer than its natural Zn-O distances, whereas Sn (Ga) in a-In-X-O allows only for shorter (longer) distances with oxygen atoms than the corresponding natural distances. In contrast, the Ge-O distances in a-InGeO exhibit the least deviation from the natural distance, as one should expect from the strong Ge-O bonds.

The deviation of the X-O distances from the natural X-O bond length may determine the connectivity between the XO_x polyhedra. For example, long X-O distances may lead to a formation of chains of connected XO_x polyhedra, whereas short X-O distance may limit the connectivity between the XO_x polyhedra or promote clustering of the XO_x polyhedra, to be discussed in Sec. IV B 3. Here we stress the importance of the connectivity of the XO_x polyhedra which may affect (i) the degree of amorphization of the In-based matrix due to a specific spatial distribution of X; (ii) the carrier mobility controlled by the scattering on XO_x clusters or nanocrystalline inclusions; and (iii) the mechanical properties of the amorphous oxides and/or the electrical properties in oxides under an external strain.

3. In-O coordination in amorphous In-O and In-X-O

The effective coordination number (ECN) can be calculated based on the obtained pair correlation function [cf., Eq. (1)] for every In atom in the cell:

$$ECN = \sum_i \exp\left[1 - \left(\frac{l_i}{l_{av}}\right)^6\right]. \qquad (2)$$

In all In-based amorphous oxides, indium is undercoordinated with oxygen atoms, Fig. 3, as compared to the c-In_2O_3 with six-coordinated In atoms, that is InO_6 polyhedra. Moreover, at 20% substitution, all X additions considered in this work have little effect on the average In-O coordination increasing it only slightly with respect to $\langle ECN \rangle = 5.0$ in a-In-O: Zn, Ga, and Sn result in $\langle ECN \rangle \sim 5.1$, whereas Ge increases it further to $\langle ECN \rangle \sim 5.3$. This is consistent with the longer average In-O distances in a-In-X-O, discussed in Sec. IV A 1. Notably, the average effective coordination number is increased to 5.4 for the In atoms which do not have a Zn neighbor in the second shell, i.e., those located away from Zn in a-IZO, Table I.
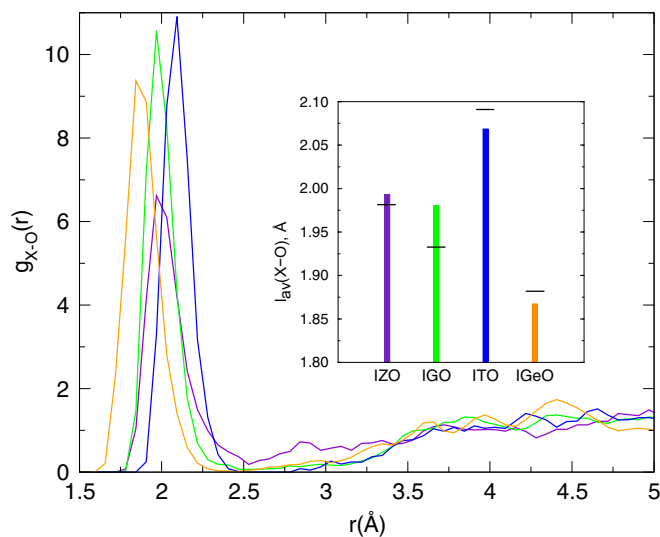

FIG. 2. (Color online) Radial pair distribution function of X-O in amorphous In-X-O. The inset shows the average X-O correlation function, l_{av}, in amorphous In-X-O; black bar lines represent the average X-O distance in the corresponding crystalline binary oxides.
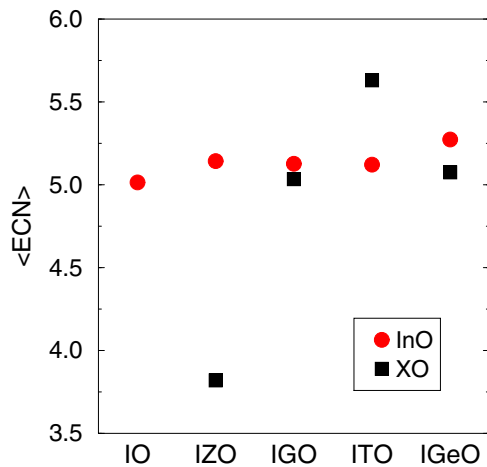
FIG. 3. (Color online) Average effective coordination number for In-O and X-O in amorphous In-O and In-X-O calculated according to Eq. (2).

To determine the origin of the increased average In-O coordination in a-In-X-O, the coordination of every In atom is calculated within a sphere of radius 2.36 Å (this is ~5% longer than the longest first-shell In-O distance in c-In$_2$O$_3$, 2.25 Å). The number of differently coordinated In atoms gives statistical distribution of the In coordinations in each system. There are three-, four-, five-, and six-coordinated In atoms, denoted below as InO$_x$, Fig. 4. In a-In-O and all a-In-X-O except for a-IGeO, around half of the In atoms are five-coordinated. Importantly, addition of Zn, Ga, and especially Ge results in an increase of the number of InO$_6$ and a suppression of both InO$_5$ and InO$_4$. In marked contrast, the number of InO$_6$ changes insignificantly upon Sn addition, so that the aforementioned slight increase of $\langle$ECN(In-O)$\rangle$ in a-ITO originates from a suppressed number of InO$_4$ and an increased number of InO$_5$ as compared to a-In-O.

The above distribution of differently coordinated In atoms, Fig. 4, suggests that Sn stands apart from the other additions since it has a negligible effect on the In coordination statistics. In contrast, Ga, Zn, and Ge increase the number of six-coordinated In atoms, with Ge resulting in the most pronounced tendency toward the natural In coordination.
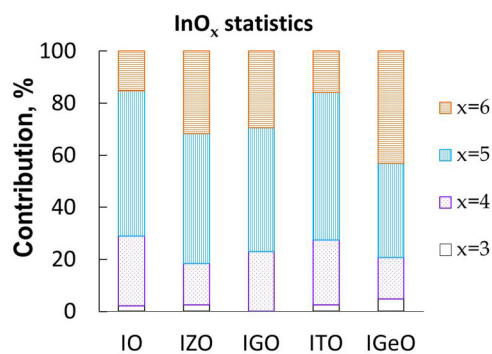

FIG. 4. (Color online) The number of differently coordinated indium atoms, InO$_x$, in amorphous In-O and In-X-O calculated within 2.36 Å around a central In atom.

These findings may be instructive to understand the role of chemical composition in carrier generation, carrier transport, and amorphization of In-based oxides (see Sec. IV B 3 below).

4. X-O coordination in amorphous In-X-O

The calculated average effective coordination number for X atoms, $\langle$ECN(X-O)$\rangle$ given in Fig. 3, reveals that the average coordination of all addition elements is close to their natural coordination, i.e., the coordination in the corresponding crystalline binary oxides—in marked contrast to undercoordinated In. Indeed, the X-O coordination calculated as an average number of oxygen neighbors within a sphere of radius r, i.e., as a function of the radial distance from a central X atom, Fig. 5, illustrates that the X atoms quickly reach and exceed their natural coordination. Moreover, statistical analysis reveals that (1) *all* Sn atoms are six-coordinated above $r = 2.36$ Å (as in crystalline SnO$_2$ and in In$_4$Sn$_3$O$_{12}$); (2) all but one Zn (9%) atom are four-coordinated above 2.24 Å (as in wurtzite ZnO and in In$_2$ZnO$_4$); (3) about a half of the Ga atoms are five-coordinated above 2.32 Å with an equal number of four- and six-coordinated Ga for the other half Ga atoms (Ga is four- and six-coordinated in β-Ga$_2$O$_3$, and five-coordinated in GaInO$_3$ and InGaZnO$_4$); and (4) about a half of Ge atoms are six-coordinated above 2.22 Å with an equal number of four- and five-coordinated Ge for the other half of Ge atoms (Ge is four-coordinated in cristobalite GeO$_2$ and in monoclinic In$_2$Ge$_2$O$_7$, and six-coordinated in rutile GeO$_2$).

We also note that Sn, Ga, and Ge average coordination reach a plateau at longer X-O radial distances, whereas Zn continues to steadily increase its coordination above the natural one—as expected from the nonvanishing Zn-O pair distribution function, Fig. 2. In marked contrast, In atoms in a-In-O remain undercoordinated even at $r = 2.6$ Å, Fig. 5. This finding suggests that In atoms remain to serve as a main source of oxygen defects upon introduction of X. We should stress, however, that the results discussed in this work are for stoichiometric oxides; the effect of oxygen nonstoichiometry (for amorphous oxides grown at different oxygen partial pressures) on the relative coordination of the constituent cations will be discussed elsewhere.

Most importantly, the structural characteristics of a-In-X-O imply that fractional substitution of indium with alternative metals does not govern the carrier generation directly. Indeed, additional cations such as Sn^{4+}, Ga^{3+}, or Zn^{2+} in amorphous indium oxide have a weak effect on the carrier concentration: at 30% X fractional substitution for In in a-In-X-O, the observed carrier concentration is measured to be 0.8×10^{20} cm^{-3}, 1.2×10^{20} cm^{-3}, and 1.6×10^{20} cm^{-3} for $X =$ Ga, Zn, and Sn, respectively. Despite the different valence of the additional cations, the resulting carrier concentrations are comparable in amorphous In-X-O and, moreover, are similar to the one observed for a-In-O, 1.6×10^{20} cm^{-3}. This implies that the X cations in amorphous oxides do not serve as dopants—in marked contrast to binary crystalline oxides where proper aliovalent external doping, e.g., Sn^{4+} on In^{3+} sites, increases the carrier concentration by orders of magnitude or to multicomponent crystalline oxides, e.g., InGaZnO$_4$, where cation substitutional disorder, Ga^{3+} on Zn^{2+}, is the major carrier donor [46].
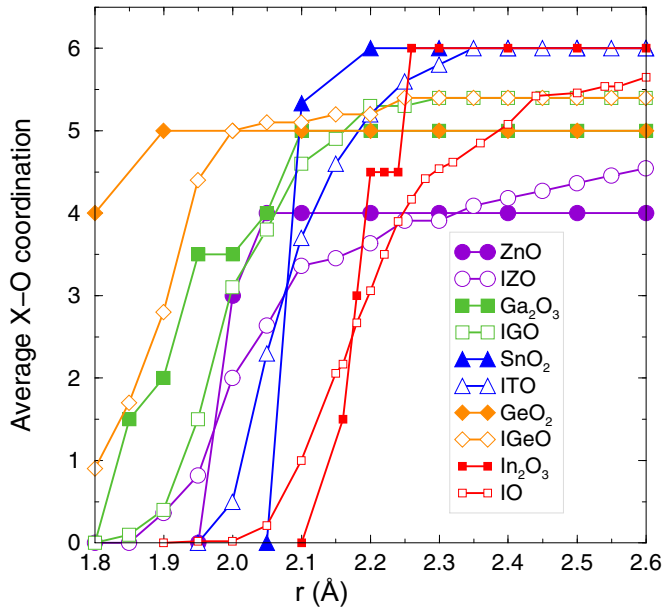
FIG. 5. (Color online) Average X-O coordination in crystalline and amorphous oxides as a function of the radial distance r, in Å, from a central X atom. Also included is the average In-O coordination in c-In$_2$O$_3$ and a-In-O. Filled (open) symbols represent crystalline (amorphous) oxides.

B. Long-range structural characteristics

1. In-M distance distribution and total In-M coordination

The analysis of the M-O (where M = In or X) bond lengths and coordination has shown that, on average, the local structure of the MO_x polyhedra remains nearly unchanged upon the transition from crystalline to amorphous state. To understand the transport properties of amorphous oxides, the long-range structural characteristics, i.e., the In-M shell distances and coordination that determine how the MO_x polyhedra are connected into a network, should be considered in great detail.

The calculated radial distribution functions for the In-M shell in a-In-O and a-In-X-O are shown in Fig. 6. The main peak in the distribution, centered at about 3.4 Å, is wide so

that it combines the second and third shells in the c-In$_2$O$_3$ associated with six edge-shared In-In bonds at ~3.35 Å and six corner-shared In-In bonds at ~3.83 Å, respectively. A suppressed third-shell peak in all amorphous oxides does not imply, however, that the total In-In coordination is reduced upon amorphization. Indeed, the total In-M coordination, calculated as a function of the distance from an In atom, Fig. 6, reaches and exceeds the expected number, 12, above 4.3 Å in amorphous In-O and In-X-O. The absence of a distinct third-shell peak in the total In-M distance distribution in amorphous oxides is due to the fact that a significant part of the edge-shared In-M pairs (about 60%) become corner-shared upon amorphization, as will be discussed in detail below; see Sec. IV B 2.

Addition of Ga or Zn increases the total In-M coordination as compared to that in a-In-O, whereas Sn slightly reduces it, Fig. 6. Importantly, the X effect on the In-M coordination is reflected not only in the In-X coordination but also in the In-In coordination which reveals a similar composition-dependent trend; see inset for Fig. 6, with lowest coordination in a-ITO and a higher coordination in amorphous IGO and IZO as compared to that of a-In-O. Although the smallest In-M coordination in a-ITO seems to be in accord with the longest average In-O distance in this oxide, the increased In-M coordination for X = Zn, Ga, or Ge cannot be explained by the first shell changes alone since the average In-O distance for these X cations also increases with respect to that in a-In-O, Fig. 1. Hence, it is necessary to further analyze the characteristics of the In-M shell.

2. Edge- and corner-shared In-M in amorphous oxides

The proximity of the indium second and third shells (at 3.35 and 3.83 Å in c-In$_2$O$_3$) causes the corresponding pair-distribution functions to overlap in the amorphous state [10]. The total In-M distance distribution becomes over 1 Å wide, Fig. 6, making the exponential fit in the l_{av} and ECN calculations, Eqs. (1) and (2), inapplicable. It is important, however, to gain a thorough understanding of the In-M shell structure since it determines the interconnectivity between the MO_x polyhedra.
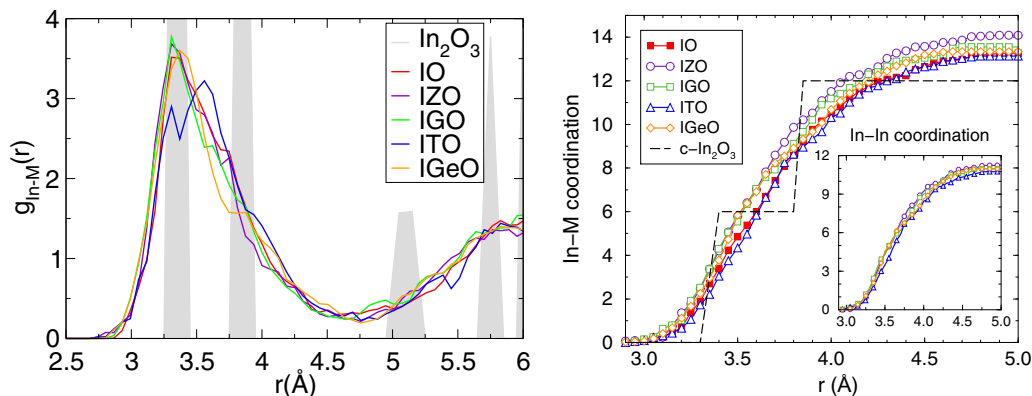

FIG. 6. (Color online) (Left) Radial In-M distribution function, $g_{In-M}(r)$, where M = In or X = Zn, Ga, Sn, Ge) as a function of distance from an In atom in crystalline In$_2$O$_3$ and in amorphous In-O and In-X-O. (Right) Total In-M coordination, where M = In or X = Zn, Ga, Sn, Ge, as a function of distance from an In atom in crystalline In$_2$O$_3$ and in amorphous In-O and In-X-O. The inset shows the In-In coordination as a function of distance for the same.
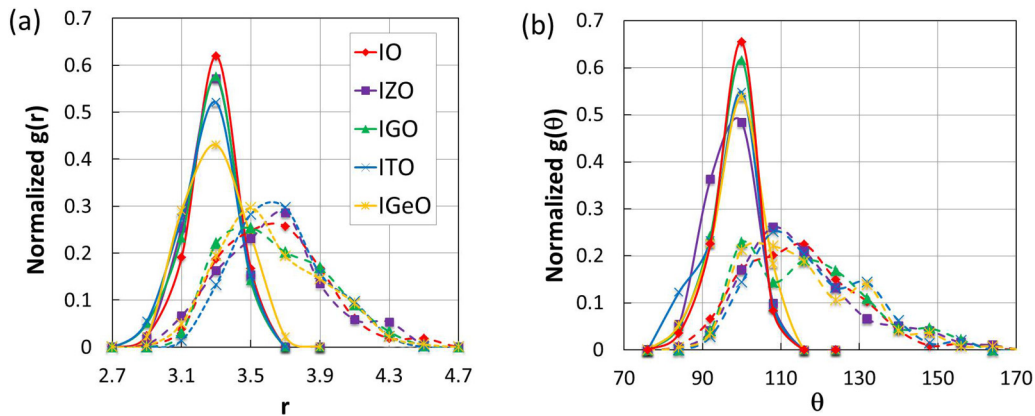
FIG. 7. (Color online) (a) Normalized In-M distance distribution functions, $g(r)$, calculated as a function of radial distance r from a central In atom, in Å, for edge-shared (solid line) and corner-shared (dash line) In-M pairs in amorphous In-O and In-X-O. (b) Normalized In-O-M angle distribution functions, $g(\theta)$, calculated for edge-shared (solid line) and corner-shared (dash line) In-M pairs.

Based on the optimized atomic coordinates of the MD simulated structures, one can distinguish between the edge- and corner-shared In-M pairs as follows. For every In atom, the number of metal neighbors (In or X) that share one, two, or three oxygen atoms with the central In atom is determined, representing the number of corner, edge, or face-shared In-M pairs, respectively. In this analysis, one should choose a maximum M-O distance to be considered as an M-O bond in the M-M sharing—this cutoff value should ensure that the first shell M-O distances in the corresponding pair distribution function (i.e., those that belong to the first In-O or X-O peak) are included into consideration. In our analysis, we set the cutoff values to 2.36 Å for the In-O bond and the Sn-O bond; 2.20 Å for the Zn-O bond and the Ga-O bond; and 2.10 Å for the Ge-O bond. The In-M distance and In-O-M angle distribution functions for both edge- and corner-shared pairs are given in Fig. 7. The important findings are as follows:

(1) The *edge-shared* In-M distances are distributed between 2.9 and 3.7 Å. For all X, the peak in the distribution function is located at $\sim$3.30 Å which is close to the second shell edge-shared In-In distance of 3.35 Å in c-In$_2$O$_3$. The width of the distribution function varies with X; the calculated standard deviation, σ^2, for the edge-shared In-M distances increases from 0.013 Å^2 for a-In-O to 0.015 Å^2 for a-IZO, to 0.020 Å^2 for a-IGO, to 0.021 Å^2 for a-ITO, and to 0.026 Å^2 for a-IGeO. The corresponding angle distribution for the edge-shared In-M pairs is from 80° to 110°, Fig. 7. The average In-O-M angle for the edge-shared In-M pairs is 98° which is slightly smaller than the corresponding edge-shared In-In angles, 99–101°, in c-In$_2$O$_3$. For a-In-O and all a-In-X-O, the average edge-shared In-M coordination saturates at $\sim$3.9 Å, as expected from the In-M distance distribution function. Comparing the values at the saturation, we find that all X cations increase the edge-shared In-M coordination, namely, from 1.62 for a-In-O to 1.66 in a-ITO, to 2.07 in a-IZO, to 2.11 in a-IGeO, and to 2.25 in a-IGaO. The improved edge-shared In-M coordination in a-In-X-O does not translate into better mobility: the observed mobility in a-In-X-O, X = Zn, Ga, or Sn, decreases as the substitutional fraction of X increases (see Sec. IV B 3). Indeed, from the structural analyses of several a-In-O structures—obtained both theoretically (modelled via

different cooling rates in MD simulations) and experimentally (deposited at different temperatures and characterized by EXAFS)—a seemingly counterintuitive conclusion was reached: the observed mobility peak corresponds to the structure with the *smallest* edge-shared In-In coordination number [10].

(2) The *corner-shared* In-M distribution function is almost two times wider compared to the edge-shared one and begins at around 3.0 Å. Such significant overlap between the two distribution functions, Fig. 7, highlights the challenge to distinguish between the second and third shells from a general pair distribution function, whether it is obtained experimentally or theoretically. The average corner-shared In-M distance is about 3.6 Å for all a-In-X-O structures which is smaller than the crystalline corner-shared In-In distance of 3.8 Å. Consequently, the corresponding angle distribution for the corner-shared In-M pairs is wide and also overlaps with the angle values for the edge-shared In-M pairs, Fig. 7. The average In-O-M angle for the corner-shared In-M pairs is 116° for a-IXO, to be compared to 126° in c-In$_2$O$_3$.

The average edge/corner-shared In-M distance and In-O-M angle do not reveal significant differences between a-In-X-O, Fig. 7. The effect of composition becomes pronounced once the corresponding values are calculated separately for In-In, In-X, and X-X pairs. Moreover, following recent findings [10] on the importance of the connectivity of six-coordinated In atoms, denoted below as In$_6$, the average distances and angles for edge and corner-shared In$_6$-In$_6$ pairs are also calculated and compared with those for the In-In pairs of all coordinations.

In-In: First, the average In-In values are calculated independently of the In coordination with oxygen atoms, i.e., for any two In atoms that are connected via edge or corner sharing. (Note, that In is primarily five-coordinated in a-In-O and in a-In-X-O except for a-IGeO, Fig. 4). The composition of ternary oxides does not change the relative number of the edge- vs corner-shared In-In pairs which remains nearly the same in a-In-O and all a-In-X-O, namely, 20% vs 80%, respectively, of the total shared In-In pairs in each oxide, Fig. 8(a). Moreover, the presence of X has little effect on the average edge-shared In-In distance as compared to the corresponding values in a-In-O, Fig. 8(c). In a-ITO, the shortest average edge-shared
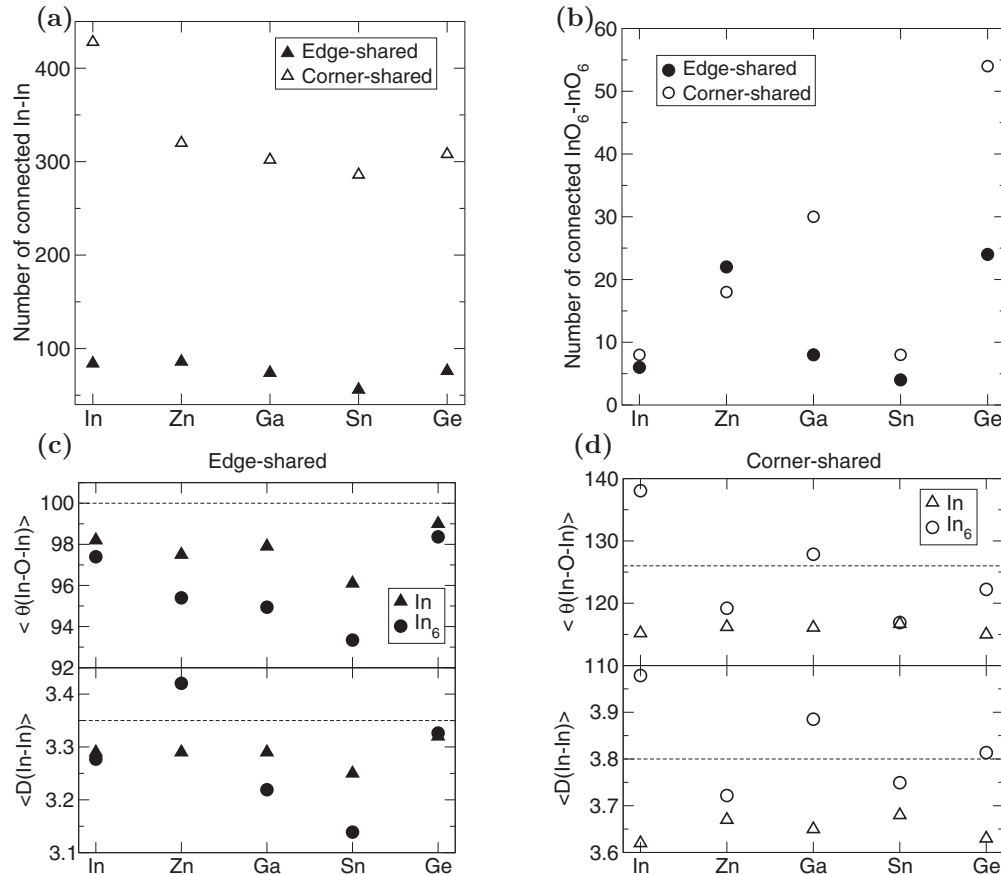
FIG. 8. Number of edge-shared and corner-shared (a) In-In pairs and (b) In_6-In_6 pairs in amorphous In-O and In-X-O. Average In-In (triangle) or In_6-In_6 (circle) distance, in Å, and average In-O-In (triangle) or In_6-O-In_6 (circle) angle, in degrees, for the InO_x or InO_6 polyhedra connected via (c) edge sharing or (d) corner sharing in amorphous In-O and In-X-O. The horizontal dash line represents the corresponding values averaged for the second and third shells in crystalline In_2O_3.

In-In distance (3.25 Å) may be due to the abundance and clustering of SnO_6 polyhedra (see Sec. IV B 3); whereas in a-IGeO, the longest edge-shared In-In distance (3.33 Å) is likely to be due to the large number of In_6 (cf., Fig. 4). The average corner-shared In-In distance increases slightly in all a-In-X-O, Fig. 8(d).

In_6-In_6: Most strikingly, the distances, angles, and connectivity between the naturally coordinated In atoms vary significantly with composition of a-In-X-O. For X = Zn, Ga, or Ge, the number of In_6 increases, whereas Sn does not affect it, Fig. 4. However, all X cations modify the way the InO_6 polyhedra connect with each other. The relative number of edge- vs corner-shared In_6-In_6 pairs, shown in Fig. 8(b), is different in a-In-X-O—in contrast to the corresponding numbers of the shared In-In pairs, Fig. 8(a). Specifically, although Sn has little effect on the fractional number of In_6, Fig. 4, it suppresses the number of edge-shared InO_6 polyhedra, Fig. 8(b). At the same time, Sn leads to the formation of short-distant edge-shared In_6 pairs (∼3.1 Å); the average corner-shared In_6-In_6 is also reduced in a-ITO as compared to a-In-O, resulting in the smallest average distance between the connected In_6-In_6 among the amorphous oxides considered. On the contrary, addition of Zn results in the longest edge-shared In_6-In_6 distance (3.42 Å) that is larger than that for the second shell in the crystalline In_2O_3, Fig. 8(c).

Moreover, only in a-IZO, the number of edge-shared InO_6 polyhedra is greater than that for the corner-shared InO_6, Fig. 8(b). Comparing a-IZO and a-IGO, the difference in the effect of composition on the InO_6 connectivity is manifested most clearly. In these oxides, the relative number of In_6 is nearly the same (and is doubled as compared to a-In-O and a-ITO, Fig. 4); the number of connected InO_6 polyhedra increases accordingly. However, Zn promotes edge sharing between the InO_6 polyhedra whereas Ga favors their corner sharing, Fig. 8. As a result, a-IZO (a-IGO) exhibits the longest edge-shared (corner-shared) In_6-In_6 distance for the connected InO_6 polyhedra among all a-In-X-O considered. Such differences in the InO_6 connectivity are likely to reflect differences in the charge transport in a-IZO and a-IGO. The spatial distribution of InO_6 polyhedra will be discussed in the next section. Finally, Ge addition results in the largest number of InO_6 polyhedra, Fig. 4, so that the edge-shared distances and angles for In-In and In_6-In_6 pairs are nearly identical and are closest to the corresponding average edge-shared values in c-In_2O_3, 3.35 Å and 100°. The average corner-shared In_6-In_6 distance also matches that in c-In_2O_3. We note that the proximity of the average In-In distance to that in c-In_2O_3 may serve as a signature of a large fraction of InO_6 polyhedra and may point out to a low effectiveness of Ge addition to amorphize indium oxide.
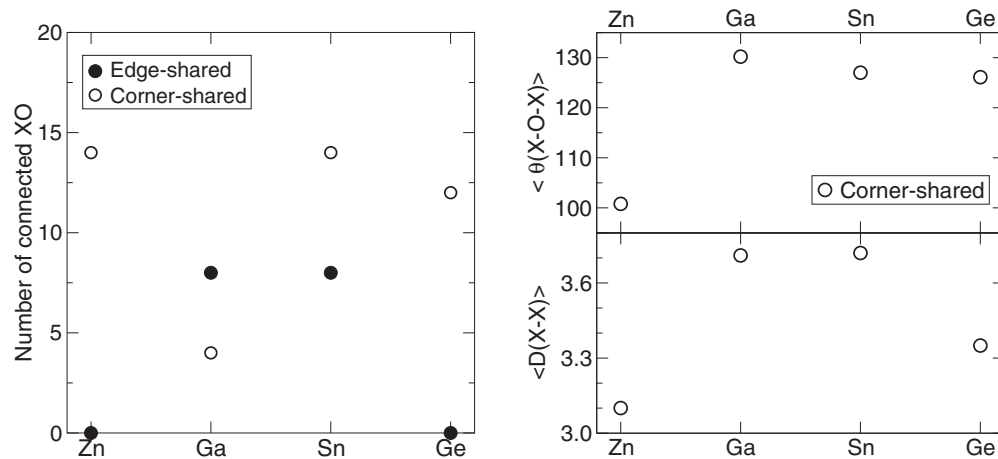
FIG. 9. (Left) Number of edge-shared and corner-shared X-X pairs in a-In-X-O. (Right) Average X-X distance, in Å, and average X-O-X angle, in degrees, for the XO_x polyhedra connected via corner sharing in amorphous In-X-O. The corresponding values for edge-shared X-X pairs for $X =$ Sn and Ga are given in the text.

In-X: The connectivity between the InO_x and XO_x polyhedra is represented by the number of the edge- vs corner-shared In-X pairs and that is affected by the X preferred coordination discussed in Sec. IV A 4 above. In particular, we find that most of the Sn and Ge atoms are six-coordinated with oxygen atoms that matches well with the framework InO_x polyhedra. Accordingly, the number of the edge- vs corner-shared In-X pairs does not change in a-ITO and a-IGeO and remains at 20% vs 80% which is similar to the corresponding ratio for In-In pairs. In marked contrast to Sn or Ge, Zn suppresses the edge-shared In-Zn number to as low as 6%. Most of the Zn atoms in a-IZO satisfy their natural coordination with oxygen atoms and, hence, such ZnO_4 polyhedra prefer only corner sharing with nearby polyhedra (as indeed, found in crystalline ZnO and In_2ZnO_4). In a-IGO, about a half of the Ga atoms are five-coordinated which is not the natural coordination for binary Ga_2O_3 but can be found in ternary and quaternary oxides. In amorphous structure, such five-coordinated Ga atoms can either share an additional oxygen atom (to become nearly six-coordinated) or let one of them loose (to become nearly four-coordinated). Both cases favor edge sharing with neighboring polyhedra. Indeed, Ga increases the number of the edge-shared In-Ga up to 30%.

X-X: The preference for the natural X-X distances, X-O-X angles, and sharing between XO_x polyhedra is evident from Fig. 9: no edge-shared Zn-Zn or Ge-Ge pairs are found in a-IZO and a-IGeO, in agreement with 100% corner sharing in crystalline binary (wurtzite ZnO and cristobalite GeO_2) as well as ternary (In_2ZnO_4 and $In_2Ge_2O_7$) oxides. Moreover, the average corner-shared X-X distances and X-O-X angles in a-IZO and a-IGeO, Fig. 9, follow those in the crystalline binary oxides, namely 3.23 Å and 110° in wurtzite ZnO or 3.43 Å and 130° in rutile GeO_2. Similarly, Sn and Ga attain their preferred distances, angles, and polyhedra sharing in the a-In-X-O: in marked contrast to Zn and Ge, both Sn and Ga favor edge sharing leading to an increased number of the edge-shared X-X pairs to 36% and to 67%, respectively, of the total number of the shared X-X pairs. (For comparison, as mentioned above, the number of the edge-shared In-In pairs does not exceed 20% in a-In-O and a-In-X-O). Consequently,

the average edge-shared Ga-Ga distance (3.02 Å) and the average edge-shared Ga-O-Ga angle (97.8°) in a-IGO are close to those in crystalline β-Ga_2O_3, 3.08 Å and 98.6°. Similarly, the average corner-shared Sn-Sn distance (3.72 Å) and the average corner-shared Sn-O-Sn angle (127.0°) in a-ITO nearly match those in crystalline SnO_2, 3.71 Å and 129.3°. The minority edge-shared Sn-Sn values are 3.33 Å and 102.8° which are comparable to 3.19 Å and 101.5° in c-SnO_2.

Thus, at 20% fractional substitution of indium atoms with X, XO_x polyhedra show a strong preference to connect with each other in the way they do in the crystalline binary counterparts. This finding suggests that the spatial distribution of the XO_x polyhedra is an important issue from the points of view of (1) amorphization, e.g., formation of nanocrystalline inclusions, and (2) electron mobility governed by charge scattering, as will be discussed in the next section. It should be stressed that oxygen nonstoichiometry may affect the coordination of both In and X atoms and, therefore, may modify the interconnectivity and spatial distribution of the InO_x and XO_x polyhedra.

3. InO_6 and XO_x spatial distribution

As mentioned in the Introduction, the size and distribution of nanocrystalline In_2O_3 inclusions which are present in the amorphous oxide samples even below the transition to the so-called x-ray amorphous state of indium oxide limit the transport properties via scattering [10]. In Fig. 4, Sec. IV A 3, the relative number of fully coordinated In atoms are given for a-In-O and a-In-X-O, and their connectivity via edge vs corner sharing is discussed in the previous section. However, the spatial distribution of the InO_6, i.e., homogeneous distribution of separate-standing (not connected) polyhedra vs chains vs clusters ultimately determines the properties [10] and should be addressed. The spatial behavior of XO_x polyhedra plays as important role and is also discussed below. In this work, the MD quench rates employed for a-In-O and a-In-X-O (170 K/ps) are expected to be fast enough to prevent InO_6 clustering and, hence, to avoid nucleation of In_2O_3 nanocrystallites observed in amorphous structures obtained at 5 K/ps

rates [10]. Indeed, in a-In-O obtained at this cooling rate, only 13% of In atoms are six-coordinated, and these InO_6 are distributed uniformly throughout the cell volume: the number of connected InO_6 (via edge or corner sharing) is small, Fig. 8, and the average distance between shared InO_6 polyhedra is 3.68 Å which is greater than the average shared In-In distance in c-In_2O_3, 3.6 Å. The latter is primarily due to the presence of long-distance corner-shared In_6-In_6 pairs that result in the average corner-shared In_6-O-In_6 angle of 138°, Fig. 8 (to compare, the average corner-shared In-O-In angle in c-In_2O_3 is 126°). All X cations considered in this work reduce the average corner-shared In_6-In_6 distance in a-In-X-O as compared to that in a-In-O, Fig. 8(d). This finding may point to a suppressed connectivity between the InO_6 polyhedra. Since the decrease does not follow the trend in the fractional number of In_6 (cf., Fig. 4), different composition-dependent mechanisms should be responsible for the formation of the amorphous oxide structure, e.g., a tendency toward InO_6 clustering may be expected in some a-In-X-O. To analyze this, the number of In_6 neighbors to a central In_6 was calculated within a radial cutoff distance of 3.8 Å. (Note that oxygen sharing, i.e., connectivity between the InO_6 polyhedra, was not taken into account in these calculations, and the distance of 3.8 Å is simply to include the In-In distance of the second and third shells in c-In_2O_3). The results are grouped according to the fractional number of six-coordinated In atoms in different compounds (cf., Fig. 4) for comparison. We find that addition of Sn reduces the probability of a single-standing InO_6 polyhedra (i.e., not connected with another InO_6) as compared to a-In-O, Fig 10. Addition of Zn completely suppresses isolated InO_6 polyhedra in a-IZO. Comparing a-IGO and a-IZO where the fractional number of In_6 atoms is the same (about 30%, Fig. 4), the
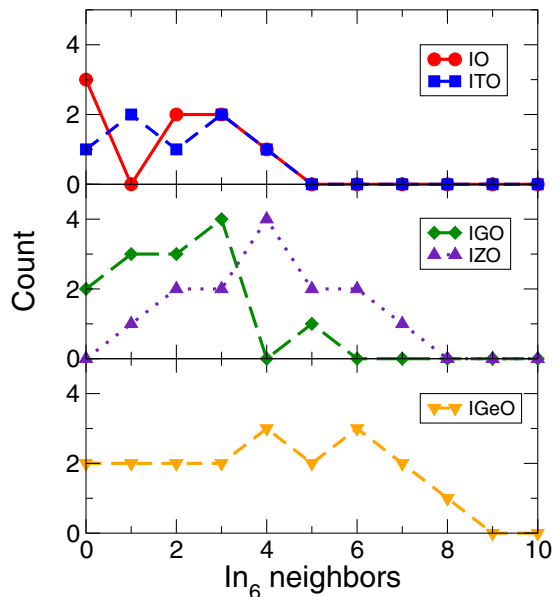

FIG. 10. (Color online) The number of In_6 neighbors calculated within a radial cutoff distance of 3.8 Å from a central In_6 in a-In-O and a-In-X-O. The oxides are grouped according to the fractional number of the six-coordinated In atoms, cf., Fig. 4, that is ~20% for a-In-O and a-ITO; ~30% for a-IGO, and a-IZO; and ~40% for a-IGeO.

different spatial distribution of the InO_6 polyhedra in these oxides is apparent, Fig. 10. In a-IGO, the In_6 atoms have primarily no, one, two or three In_6 neighbors; a single cluster of five InO_6 neighbors is observed. In contrast, a-IZO has a bell-shape distribution of the In_6 neighbors with four In_6 neighbors to be the most likely arrangement, Fig. 10. Such preferential distribution of the six-coordinate In atoms in a-IZO is likely due to the strong tendency of Zn to facilitate edge sharing between the In_6 atoms, Fig. 8(b), thus forming long continuous chains of shared InO_6 polyhedra in a-IZO. Finally, the number of InO_6 is largest in a-IGeO, Fig. 4, and the probability to find an In_6 cluster of any size (no or one to eight neighbors) is nearly the same in a-IGeO. This indifference to the In_6 cluster size in a-IGeO may arise from the smallest ionic radius of Ge among the X atoms considered, and signify the inability of the Ge addition to amorphize In-based oxides. We must stress here that the role of oxygen nonstoichiometry and deposition temperatures (or cooling rates) on the structural properties of a-In-X-O was not taken into account in this work. Such investigations are ongoing and are expected to elaborate on the effect of X addition. In ternary In-based amorphous oxides, the spatial distribution and connectivity of XO_x polyhedra are expected to have a greater effect on the charge scattering than the distribution of InO_6 polyhedra discussed above. The strong tendency of X atoms toward their natural distances in first, second, and third shells as well as toward the type of sharing between the XO_x polyhedra have been demonstrated in Sec. IV A 2. At 20% fractional substitution, we observe that the number of shared XO_x polyhedra correlates with the X ionic radius: for X = Zn, Ga, or Ge with smaller ionic radii there are 12–14 X-X connections per cell, whereas for the larger Sn addition, the total number of Sn-Sn connections increases to 22, Fig. 9. Although the number of connected XO_x polyhedra is similar in amorphous IZO, IGO, and IGeO, the strong preference for edge sharing between the GaO_x polyhedra leads to the formation of GaO_x clusters in a-IGO—in marked contrast to a more homogeneous distribution of ZnO_x and GeO_x polyhedra in the respective oxides, as discussed in the next section. Most strikingly, a-ITO features significant SnO_x clustering having eight SnO_6 polyhedra connected via edge sharing with the rest of the SnO_6 polyhedra attached to the cluster via corner sharing. This finding may be explained by the large Sn ionic size and its strong ability to attain full coordination with oxygen atoms as compared to more distortion-tolerant In atoms. This finding resembles the structural characteristics of crystalline $In_4Sn_3O_{12}$ where a fraction of Sn atoms form regular SnO_6 polyhedra, whereas the rest of the Sn atoms and all In atoms have a low-symmetry coordination with the In/Sn-O distances ranging from 2.07 to 2.31 Å. Thus, Sn addition may help attain amorphous In-based oxide structure by distorting the InO_x polyhedra and, hence, may help prevent InO_6 clustering with subsequent formation of In_2O_3 nanocrystallites. On the other hand, Sn has a strong tendency to cluster itself which ultimately limits the electron mobility as the fraction of Sn increases. Indeed, among the PLD-grown amorphous In-X-O with X = Zn, Ga, and Sn, the observed carrier mobility of a-ITO is highest only up to about 10% of the Sn fractional substitution, Fig. 11. The mobility drops significantly for larger Sn fraction, and above 15% becomes lower than that in a-IZO
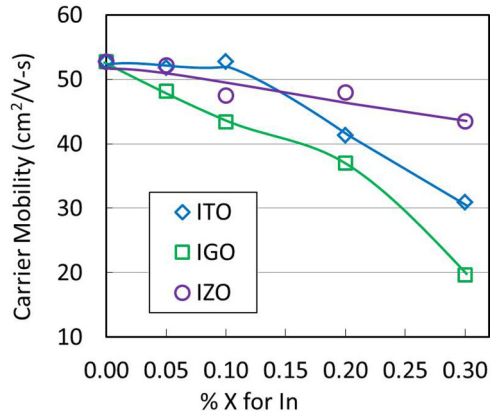
FIG. 11. (Color online) Observed Hall mobility in PLD-grown amorphous In-X-O, X = Zn, Ga, or Sn, as a function of fractional substitution.

where no Zn clustering was found from the MD simulations. A similar behavior of the carrier mobility is observed in a-IGO where a change in the slope occurs at about 20% of Ga

substitution for In, Fig. 11, signifying a stronger scattering possibly associated with an onset of GaO$_x$ clustering that was found in our MD-simulated a-IGO structure. The linear decrease of the carrier mobility with Zn fractional substitution is in accord with the proposed uniform distribution of ZnO$_x$ throughout the InO$_x$ framework.

C. Structural models of amorphous In-X-O

The above comparison of the local and long-range structural characteristics of amorphous In-X-O points to the substantial differences between the oxides that originate from the different ionic size, valence, metal-oxygen bond strength, and oxygen-sharing preferences of the cations. To illustrate the different structural behavior in the amorphous In-X-O oxides, their atomic structures are presented in Fig. 12 where both the InO$_6$ and XO$_x$ polyhedra are highlighted. Based on the results of MD simulations, we propose the following structural models of amorphous In-X-O that help explain the observed transport properties in these oxides (Fig. 11).

In a-IZO, Zn exhibits both longer and shorter than the natural Zn-O distances resulting in a wide Zn-O pair distribution.
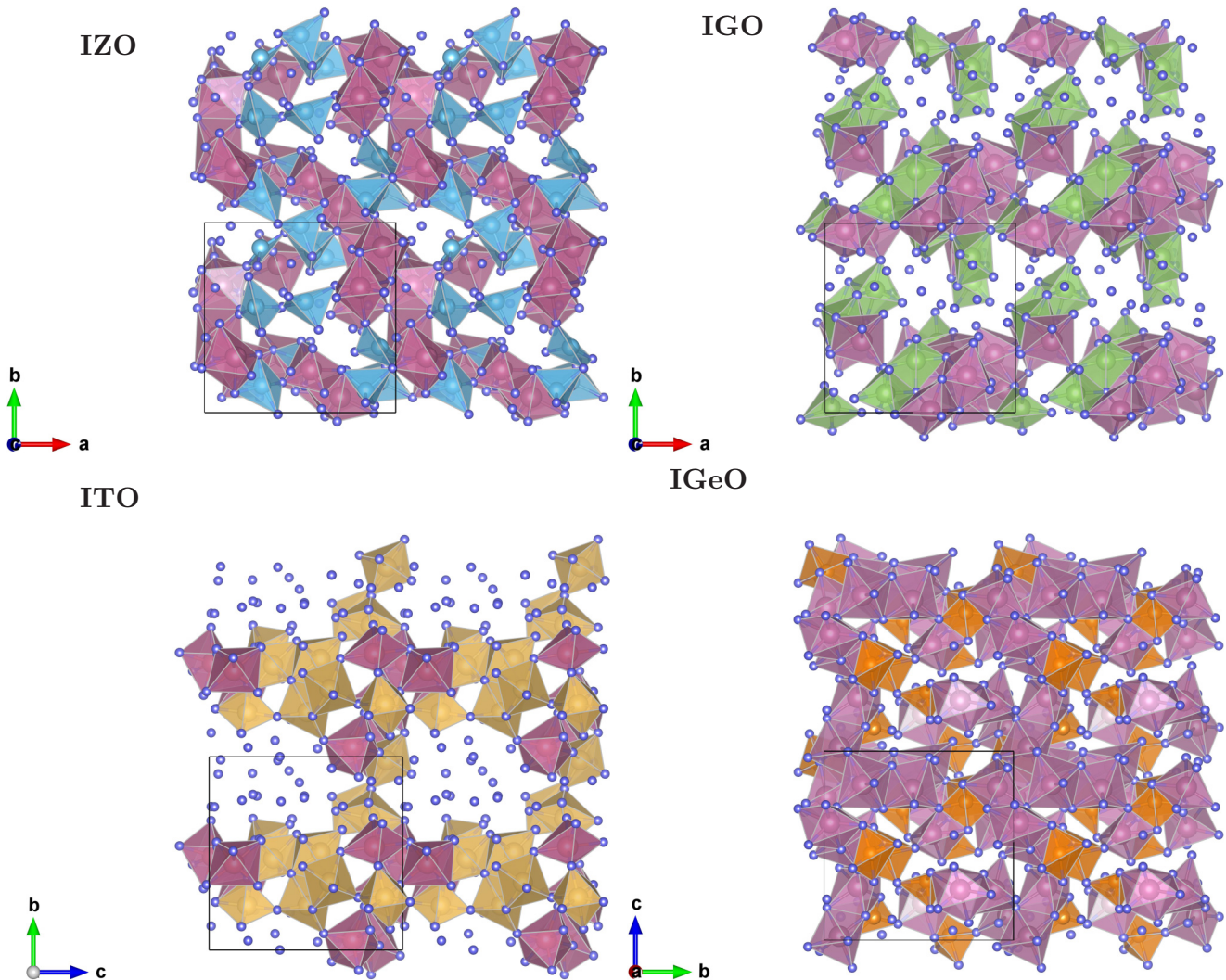

FIG. 12. (Color online) Atomic structures of a-In-X-O, X = Zn, Ga, Sn, or Ge, highlighting the InO$_6$ and XO$_x$ polyhedra only. Small spheres represent oxygen atoms, and large spheres represent In or X atoms.

This points out the ability of Zn to adopt to the distortions of amorphous environment—a property that is advantageous in the oxides under strain. Addition of Zn increases the coordination of In atoms located away from Zn and strongly favors edge sharing between InO_6 polyhedra. The latter form long connected chains that serve as conductivity paths, Fig. 12. At the same time, Zn maintains its tetrahedral coordination with oxygen that ensures corner sharing of ZnO_x polyhedra and facilitates a uniform distribution of the ZnO_x polyhedra throughout the InO_x framework, Fig. 12. Absence of ZnO_x clustering mitigates charge scattering in a-IZO, in accord with the measured linear dependence of the mobility with Zn fractional substitution, Fig. 11. Hence, the long chain network of InO_6 supported by ZnO_4 gives rise to the excellent carrier mobility observed in a-IZO.

In a-ITO, addition of Sn does not affect the InO_x coordination statistics, in agreement with the unchanged carrier concentration of a-ITO at 30% Sn substitution as compared to the one observed for a-In-O (1.6×10^{20} cm^{-3} for both cases). Moreover, the presence of Sn does not affect the spatial distribution and sharing between the InO_6 polyhedra as compared to a-In-O. At the same time, Sn satisfies its natural distances and coordination with oxygen. Strikingly, these SnO_6 polyhedra fill the space between disconnected InO_6 polyhedra, and together they form a distinct network of long connected chains, Fig. 12. Given the electronic similarities between the six-coordinate In and Sn ions, such InO_6-SnO_6 chains are expected to serve as conductivity paths for good charge transport. Indeed, the carrier mobility remains constant in a-ITO up to 10% Sn fractional substitution, Fig. 11. At larger Sn concentrations, the strong tendency of Sn to cluster causes electron scattering so that the carrier mobility decreases rapidly above 10% Sn fractional substitution in a-ITO.

In a-IGO, Ga cations, on average, satisfy their natural coordination with oxygen, adopting a four-, five- or six-fold local oxygen environment. As a result of the sustained multi-coordination, Ga suppresses the number of low-coordinated In atoms in a-IGO which may explain the largest reduction of the observed carrier concentration with fractional Ga substitution as compared to a-ITO and a-IZO. Addition of Ga triples the number of corner-shared InO_6 polyhedra and has no effect on the number of edge-shared In_6 pairs. Hence, Ga helps prevent growth of nanocrystalline In_2O_3 inclusions that makes Ga cation an effective candidate for amorphization of indium oxide. However, the absence of extended InO_6 chains along with a strong charge scattering associated with clusters of the edge-shared GaO_x polyhedra, Fig. 12, is expected to limit the electron transport in a-IGO as the Ga fractional substitution increases.

In a-IGeO, owing to the strong Ge-O bonds, the average Ge-O distance and Ge coordination with oxygen remain at their natural values. Ge nearly triples the fractional number of six-coordinated indium atoms as compared to the a-In-O and increases the average distance between edge- and corner-shared In_6 pairs to nearly crystalline In_2O_3 values. Hence, Ge addition facilitates the formation and growth of nanocrystalline indium oxide and is likely to limit the ability of a-IGeO to generate carriers.

V. CONCLUSIONS

The results of *ab initio* molecular-dynamics liquid-quench simulations of ternary In-based amorphous oxides, a-In-X-O with $X =$ Sn, Zn, Ga, or Ge, reveal that an interplay between the local and long-range structural preferences of the constituent oxides gives rise to a complex composition-dependent behavior in these multicomponent materials. More specifically, it is found that the local structure of the MO_x polyhedra remains, on average, nearly unchanged upon the transition from crystalline to amorphous state. Moreover, the average In-O coordination is 5.0–5.2 in a-In-O and all a-In-X-O considered in this work. Such a weak dependence of the In coordination on the composition signifies that In atoms remain to serve as a main source of oxygen defects upon fractional substitution with X. This is in accord with a similar carrier concentration measured for amorphous In-O (1.6×10^{20} cm^{-3}) and for In-X-O at 30% substitution with $X =$ Ga, Zn, or Sn (0.8, 1.2, or 1.6×10^{20} cm^{-3}, respectively). Hence, in marked contrast to crystalline transparent conducting oxides, the additional cations in amorphous oxides do not serve as dopants and do not govern the carrier generation directly. At the same time, composition-induced differences in the connectivity and spatial distribution of InO_6 and XO_x polyhedra determine the formation of the amorphous structures as well as the carrier mobility which is controlled by electron scattering. Based on the structural results of the MD simulations, the proposed composition-dependent models of amorphous oxide network help explain the observed electrical properties in amorphous In-O-X. These systematic results shed light on the role of composition in tuning the properties of amorphous oxides and facilitate the progress in fundamental understanding of amorphous transparent conducting oxides.

ACKNOWLEDGMENTS

[1] J. Bellingham, W. Phillips, and C. Adkins, J. Phys.: Condens. Matter. **2**, 6207 (1990).

[2] H. Hosono, M. Yasukawa, and H. Kawazoe, J. Non-Cryst. Solids **203**, 334 (1996).

[3] K. Nomura, H. Ohta, A. Takagi, T. Kamiya, M. Hirano, and H. Hosono, Nature (London) **432**, 488 (2004).

[4] D. Ginley, H. Hosono, and D. Paine, *Handbook of Transparent Conductors* (Springer, New York, 2010).

[5] J. Perkins, M. van Hest, C. Teplin, J. Alleman, M. Dabney, L. Gedvilas, B. Keyes, B. To, D. Ginley, M. Taylor, *et al.*, in *Photovoltaic Energy Conversion, Conference Record of the 2006 IEEE 4th World Conference on* (Waikoloa, Hawaii, 2006), Vol. 1, pp. 202–204.

[6] K. Ghaffarzadeh and R. Das, technical report, IDTechEx, 2014 (unpublished).

[7] D.-Y. Cho, N. J. Song, C. Hwang, J. Jeong, J. Jeong, and Y.-G. Mo, Appl. Phys. Lett. **94**, 112112 (2009).

[8] C. Hoel, S. Xie, C. Benmore, C. Malliakas, J.-F. Gaillard, and K. Poeppelmeier, Z. Anorg. Allg. Chem. **637**, 885 (2011).

[9] D. Proffit, Q. Ma, D. Buchholz, R. Chang, M. Bedzyk, and T. Mason, J. Am. Ceram. Soc. **95**, 3657 (2012).

[10] D. Buchholz, Q. Ma, D. Alducin, A. Ponce, M. Yacaman, R. Khanal, J. Medvedeva, and R. Chang, Chem. Mater. **26**, 5401 (2014).

[11] K. Nomura, T. Kamiya, H. Ohta, T. Uruga, M. Hirano, and H. Hosono, Phys. Rev. B **75**, 035212 (2007).

[12] J. Rosen and O. Warschkow, Phys. Rev. B **80**, 115215 (2009).

[13] A. Walsh, J. D. Silva, and S.-H. Wei, Chem. Mater. **21**, 5119 (2009).

[14] A. Aliano, A. Catellani, and G. Cicero, Appl. Phys. Lett. **99**, 211913 (2011).

[15] S. Davis and G. Gutierrez, J. Phys.: Condens. Matter **23**, 495401 (2011).

[16] M. Kim, I. Kang, and C. Park, Curr. Appl. Phys. **12**, S25 (2012).

[17] K. Nishio, T. Miyazaki, and H. Nakamura, Phys. Rev. Lett. **111**, 155502 (2013).

[18] M. Ramzan, T. Kaewmaraya, and R. Ahuja, Appl. Phys. Lett. **103**, 072113 (2013).

[19] H.-X. Deng, S.-H. Wei, S.-S. Li, J. Li, and A. Walsh, Phys. Rev. B **87**, 125203 (2013).

[20] P. P. Zawadzki, J. Perkins, and S. Lany, Phys. Rev. B **90**, 094203 (2014).

[21] J. Medvedeva, Europhys. Lett. **78**, 57004 (2007).

[22] J. E. Medvedeva and C. L. Hettiarachchi, Phys. Rev. B **81**, 125116 (2010).

[23] A. Murat and J. E. Medvedeva, Phys. Rev. B **85**, 155101 (2012).

[24] J. Medvedeva and A. Freeman, Europhys. Lett. **69**, 583 (2005).

[25] J. Medvedeva, Appl. Phys. A **89**, 43 (2007).

[26] J. Medvedeva, *in Transparent Electronics: From Synthesis to Applications* (John Wiley & Sons, 2010), pp. 1–29.

[27] T. Kamiya, K. Nomura, M. Hirano, and H. Hosono, Phys. Status Solidi C **5**, 3098 (2008).

[28] H.-K. Noh, K. J. Chang, B. Ryu, and W.-J. Lee, Phys. Rev. B **84**, 115205 (2011).

[29] W. Körner and C. Elsässer, in *International Symposia on Transparent Conductive Materials, October 2012* [Thin Solid Films **555**, 81 (2014)].

[30] W. Körner, D. F. Urban, and C. Elsässer, Phys. Status Solidi A (2015), doi:10.1002/pssa.201431871.

[31] S. Sallis, K. T. Butler, N. F. Quackenbush, D. S. Williams, M. Junda, D. A. Fischer, J. C. Woicik, N. J. Podraza, B. E. White, A. Walsh *et al.*, Appl. Phys. Lett. **104**, 232108 (2014).

[32] W. H. Han, Y. J. Oh, K. J. Chang, and J.-S. Park, Phys. Rev. Appl. **3**, 044008 (2015).

[33] G. Kresse and J. Hafner, Phys. Rev. B **47**, 558 (1993).

[34] G. Kresse and J. Hafner, Phys. Rev. B **49**, 14251 (1994).

[35] G. Kresse and J. Furthmüller, Comput. Mater. Sci. **6**, 15 (1996).

[36] G. Kresse and J. Furthmüller, Phys. Rev. B **54**, 11169 (1996).

[37] P. Hohenberg and W. Kohn, Phys. Rev. **136**, B864 (1964).

[38] W. Kohn and L. Sham, Phys. Rev **140**, A1133 (1965).

[39] J. Perdew, K. Burke, and M. Ernzerhof, Phys. Rev. Lett. **78**, 1396 (1997).

[40] P. E. Blöchl, Phys. Rev. B **50**, 17953 (1994).

[41] G. Kresse and D. Joubert, Phys. Rev. B **59**, 1758 (1999).

[42] R. Hoppe, Angew. Chem. Int. Ed. Engl. **9**, 25 (1970).

[43] R. Hoppe, S. Voigt, H. Glaum, J. Kissel, H. Muller, and K. Bernet, J. Less-Common Met. **156**, 105 (1989).

[44] J. Hennek, J. Smith, A. Yan, M.-G. Kim, W. Zhao, V. Dravid, A. Facchetti, and T. Marks, J. Am. Chem. Soc. **135**, 10729 (2013).

[45] Inorganic Crystal Structure Database (ICSD), URL http://www.fiz-karlsruhe.de/icsd_web.html.

[46] A. Murat, A. U. Adler, T. O. Mason, and J. E. Medvedeva, J. Am. Chem. Soc. **135**, 5685 (2013).